APPARENT DIFFUSION DUE TO MOUNTAIN MICROSTRUCTURE IN SHALLOW WATERS

Andre Nachbin
[*] *Instituto de Matemática Pura e Aplicada*
Est. D. Castorina 110, Jardim Botânico
Rio de Janeiro, RJ 22460-320, Brazil
e-mail: nachbin@impa.br

Knut Sølna
[†] *Department of Mathematics, University of California, Irvine,*
Irvine, CA 92697-3875, USA
e-mail: ksolna@math.uci.edu
(September 4, 2002)

Abstract:
Wave propagation in disordered (random) media is the underlying theme. We study the effective behaviour of long coastal waves that travel over rough topographies. The topographies analyzed contain a smooth slowly varying profile together with disordered small-scale features. The mathematical model is a Conservation Law with random coefficients. The main (stochastic theory) asymptotic result is that the medium fluctuations cause the propagating pulse to broaden as it travels. The so called *apparent diffusion* (or pulse shaping) depends only on the traveling distance and the *statistics* of the random medium fluctuations. Thus, the broadening can be described in a deterministic way independently of the particular medium realization. This is confirmed numerically. Numerical experiments also show that the theory describing pulse shaping is very robust. Nonlinear shallow water simulations show that small amplitude pulse shaping is not affected by higher order terms. The robustness of the theory is observed numerically for a wide parameter regime. We vary both the microscale fluctuation level as well as the horizontal length scales of the topography. The numerical experiments produce very good results regarding the prediction for the wavefront attenuation.

I. INTRODUCTION

Wave–topography interaction has been the subject of considerable mathematical research. The physical applications range from coastal surface waves [13] to atmospheric flows over mountain ranges [2,8]. In particular, the interaction of waves with fine features of the topography is of great interest. As pointed out in the introduction to the *Orography* proceedings [8] of the European Centre for Medium-Range Weather Forecasts (ECMWF), the "representation (...) of subgrid-scale orographic processes is recognized as crucial to numerical weather prediction at all time ranges". In the atmospheric literature *orography* implies mountain ranges [2]. Our study is therefore focused on the effect of small-scale topographic features, which we call the *microstructure*. A mathematical theory is described and its robustness validated numerically.

In this paper we study the interaction due to long coastal waves traveling over a rough topography. In the future we intend to extend this study to models including the effect of rotation. As surface gravity waves propagate from deep to shallow waters, they are transformed due to shoaling, refraction, diffraction and reflection. To concentrate on the main scattering mechanism connected with the pulse shaping phenomenon described below, we consider the normal incidence of surface pulse shaped waves. These waves propagate over topographies containing a smooth slowly varying profile together with disordered (random) small-scale features. In other words, a pulse propagates in a medium whose parameters vary randomly. The mathematical model is a Conservation Law with random coefficients.

The main result is that the random medium fluctuations cause the propagating pulse to broaden as it travels. Due to multiple scattered energy, the pulse appears to diffuse about a moving center. The amount of broadening is proportional to the square root of the traveling distance. Moreover, the *apparent diffusion* depends only on the traveling distance and the *statistics* of the random medium fluctuations. Thus, the broadening can be described in a deterministic way independently of the particular medium realization. This important observation will be confirmed numerically. However the *velocity* of the wave pulse contains a small *random* component. In the sequel we refer to the transformation of the pulse, due to the microscale medium fluctuations, as *pulse shaping*. It is worth noticing that effective medium theory is valid for short propagation distances on the scale of the wavelength. In the effective

medium regime (i.e. homogenization theory) there is no pulse shaping. In the regime that we consider, with relatively long propagation distances, the microstructure affects the pulse shape, moreover, the traveltime includes a small random component.

Through numerical experiments we show that the theory that describes the pulse shaping is very robust. Nonlinear shallow water simulations show that small amplitude pulse shaping is not affected by higher order terms. We show the robustness of the theory in a wide parameter regime, by varying both the microscale fluctuation level as well as the horizontal length scales. This is important for the theory to be useful in a range of applications.

The theory for pulse shaping was originally derived in the context of acoustic wave propagation in the earth's crust [18]. For such a medium one of the authors has analyzed the spreading of an acoustic pulse due to the microscale variations in the medium parameters (Papanicolaou & Sølna [19]; Sølna [20]). The motivation for modeling in terms of a random medium is that a detailed description of microscale medium fluctuations are often not known. Using a stochastic model uncertainties about a specific medium are translated into uncertainties about a transmitted pulse shape in a systematic way [1,4,5,9–12]. Moreover, typical pulse shaping can be examined and characterized. As mentioned above the broadening of the pulse traveling through the random medium can actually be described in a deterministic way, to leading order, assuming that the statistics of the random variations are known. Stochastic modeling has been used for long, weakly dispersive surface wave problems by Nachbin [14] and Nachbin & Papanicolaou [17]. It was also considered by Devillard *et al.* [7] and verified experimentally in a wavetank by Belzons *et al.* [3].

In section II we present the nonlinear shallow water model for which the numerical method we use was formulated [6]. We also introduce its linear approximation for which the pulse shaping theory is derived. In section III and IV the pulse shaping theory is described and it is validated numerically in section V. We demonstrate an excellent agreement between theory and numerical experiments in a wide parameter regime.

II. THE SHALLOW WATER MODEL

We consider gravity driven surface waves propagating in shallow channels. The regime of interest is such that the fluid is considered to be inviscid and incompressible. In particular, potential theory can be used to describe the interaction of long waves with rapidly varying features of the bottom topography [13,22].

Regarding wave–topography interaction the following characteristic length scales [22] are important in studying different regimes of propagation: the typical depth is given by h_0, the typical wavelength by λ and the typical amplitude of the free surface elevation $\eta(x,t)$ by a. We also have the horizontal length scale l_b for the bottom irregularities, as well as L representing the total length of the rough region (c.f. Figure 1). The importance of these scales becomes clear when we look at the *dimensionless* potential theory equations. The velocity potential $\phi(x,z,t)$ satisfies the dimensionless equations [22]:

$$\beta\ \phi_{xx} + \ \phi_{zz}\ =\ 0 \quad \text{for} \quad -h(x/\gamma) < z < \alpha\eta(x,t),$$

with the nonlinear free surface conditions

$$\eta_t + \alpha\phi_x\eta_x - \frac{1}{\beta}\phi_z = 0$$

$$\eta + \phi_t + \frac{\alpha}{2}\left(\phi_x^2 + \frac{1}{\beta}\phi_z^2\right) = 0$$

at $z = \alpha\eta(x,t)$. The Neumann condition at the impermeable bottom is

$$\phi_z + \frac{\beta}{\gamma}\ h'(x/\gamma)\phi_x = 0.$$

The bottom topography is described by $z = -h(x/\gamma)$. The different regimes are controlled by the dimensionless parameters $\alpha = a/h_o$, which controls the strength of nonlinearity, $\beta = h_0^2/\lambda^2$, which controls dispersion and $\gamma = l_b/\lambda$ which controls how rapidly the bottom irregularities vary. The acceleration due to gravity is denoted by g and the reference shallow water speed is $c_0 = (gh_0)^{1/2}$. Different regimes of interest can be identified through these dimensionless parameters [22]. Using this model Nachbin & Papanicolaou [14,17] studied the reflection/transmission problem for linear ($\alpha = 0$), weakly dispersive ($\beta \ll 1$) surface pulse shaped waves propagating over topographies having only disordered small-scale features ($\gamma \ll 1$).

In the present work we are interested in studying long wave interaction with topographies having two components: a smooth slowly varying *background* superimposed with rapidly varying features which we call the *microstructure*.

In the small amplitude regime ($0 < \alpha \ll 1$) we show numerically that nonlinearity is in fact a higher order effect. The pulse shaping theory is robust and, for example, long waves ($0 < \beta \ll 1$) will not break while interacting with the topography. We also point out that using potential theory and stochastic modeling, Nachbin & Papanicolaou [17,14] showed that in the presence of rapidly varying topographies, the statistics for the reflection and transmission coefficients of long waves are effectively the same as for the corresponding shallow water model (c.f. section 7 [17]). Namely the infinitesimal generator for the reflection process is the same for these two models.

In the present work we study transmitted waves and pulse shaping through a nonlinear shallow water model. As pointed out in Nachbin & Papanicolaou [17,14] its linear approximation captures the essential physical properties regarding reflection/transmission of long surface waves over disordered topographies. The presence of nonlinear terms, in the shallow water equations, permits the study of the robustness of the asymptotic theory. Moreover, Casulli & Cheng [6] developed a very efficient 3D nonlinear shallow water solver, that was kindly made available to us.

Casulli & Cheng [6] considered the following nonlinear shallow water model in order to formulate their numerical scheme. Let the horizontal x and y velocity components be given by $u(x,y,z,t)$, $v(x,y,z,t)$ and the z–vertical component by $w(x,y,z,t)$. Time is denoted by t. The system of partial differential equations for the free surface problem is given by

$$u_t + uu_x + vu_y + wu_z = -g\eta_x \tag{1}$$

$$v_t + uv_x + vv_y + wv_z = -g\eta_y \tag{2}$$

$$\eta_t + \left[\int_{-h}^{\eta} u dz\right]_x + \left[\int_{-h}^{\eta} v dz\right]_y = 0. \tag{3}$$

The vertical velocity component w is calculated from the conservation of mass equation. Further conditions were incorporated, such as viscous terms, the tangential boundary stress along the free surface and along the sediment–water interface [6]. We omit these terms and conditions since they are not going to be taken into account in our analysis and experiments. A further simplification takes place when a vertical average is taken over the water body. The model reduces to the shallow water equations

$$U_t + UU_x + VU_y = -g\eta_x \tag{4}$$

$$V_t + UV_x + VV_y = -g\eta_y \tag{5}$$

$$\eta_t + [HU]_x + [HV]_y = 0, \tag{6}$$

where the vertical averages are defined by

$$U(x,y,t) = \frac{1}{H}\int_{-h}^{\eta} u\ dz, \quad V(x,y,t) = \frac{1}{H}\int_{-h}^{\eta} v\ dz \tag{7}$$

and $H(x,y,t) = \eta(x,y,t) + h(x,y)$. In the numerical method adopted for our simulations this approximation is performed over each vertical layer of a three-dimensional grid (Casulli & Cheng [6]).

In Whitham [22] the scaling is such that the dimensionless potential $\tilde{\phi}$ is given by

$$\tilde{\phi} = \frac{c_o}{g\lambda a}\phi.$$

In the dimensionless potential theory equations given above the tilda were dropped. Using the reference potential $g\lambda a/c_o$ the horizontal velocities are scaled accordingly, along with the other variables:

$$\tilde{x} = x/\lambda, \quad \tilde{y} = y/\lambda, \quad \tilde{t} = t/T, \quad T = \lambda/c_0 \quad \text{and} \quad \tilde{\eta} = \eta/a.$$

Note that ga/c_o has dimensions of velocity ([length]/[time]). Let this be the characteristic horizontal speed and define

$$\tilde{U} = U/(ga/c_o) \quad \text{and} \quad \tilde{V} = V/(ga/c_o).$$

We get the dimensionless nonlinear shallow water system

$$\tilde{U}_{\tilde{t}} + \alpha\tilde{U}\tilde{U}_{\tilde{x}} + \alpha\tilde{V}\tilde{U}_{\tilde{y}} = -\tilde{\eta}_{\tilde{x}}$$

$$\tilde{V}_{\tilde{t}} + \alpha\tilde{U}\tilde{V}_{\tilde{x}} + \alpha\tilde{V}\tilde{V}_{\tilde{y}} = -\tilde{\eta}_{\tilde{y}}$$

$$\tilde{\eta}_{\tilde{t}} + \left[\tilde{H}\tilde{U}\right]_{\tilde{x}} + \left[\tilde{H}\tilde{V}\right]_{\tilde{y}} = 0,$$

where the body of fluid is described by

$$\tilde{H}(\tilde{x},\tilde{y},\tilde{t}) = \alpha\tilde{\eta}(\tilde{x},\tilde{y},\tilde{t}) + \tilde{h}(\tilde{x}/\gamma,\tilde{y}).$$

The topography scaling was done in the x-direction, for which we will present the pulse shaping theory.

The pulse-shaping theory to be presented is derived for the one-dimensional, linear approximation of the shallow water system given above. Namely by taking the $\alpha = 0$ regime, and going back to the original variables, we have

$$U_t + g\eta_x = 0, \tag{8}$$

$$\eta_t + [hU]_x = 0. \tag{9}$$

The mountains' microstructure is contained in the disordered, rapidly varying component of the coefficient $h(x)$. The microstructure will be modeled by piecewise constant ridges of random heights. References for the interaction of long linear waves with a stepped ridge (or trench) can be found in chapter 4 of Mei's book [13]. Alternatively the linear shallow water system can be written as

$$\Psi_t + (gh)\ \eta_x = 0 \tag{10}$$

$$\eta_t + \Psi_x = 0, \tag{11}$$

where the flux function, per unit width, is given by $\Psi(x,t) \equiv h(x)\cdot U(x,t)$. The local wave speed is $c(x) = \sqrt{gh(x)}$.

In the next section the pulse shaping theory will be described for the linear wave system presented above. We show in Section V by numerical simulations that this theory is very robust. There we carry out nonlinear shallow water simulations and show that small amplitude pulse shaping is not destroyed by higher order terms.

III. PULSE SHAPING IN LINEAR CASE

In this section we discuss the solution of the wave system (10–11) when the wave speed, $c(x) = \sqrt{gh(x)}$, fluctuates randomly corresponding to the water depth h being a random function. The fluctuations in the water depth entail that the water wave changes its shape as it travels. The system (10–11) is analogous to the model for the propagation of acoustic waves in a medium with variable density. It is well known how a travelling acoustic pulse is affected by rapid random variations in the local speed of sound. We here summarize how this interaction can be described for a particular model of the wave speed fluctuations. In the next section we present a brief argument that derives these results for how the flux function Ψ interacts with the randomness in the water depth. Then, in Section V we verify numerically that this description indeed captures very well the pulse shaping for the nonlinear shallow water model described in the previous section.

We model the wave speed as follows:

$$c^2(x) = gh(x) = c_0^2(0) \quad \text{for} \quad x < 0 \tag{12}$$

$$c^2(x) = c_0^2(x)/(1 + \sigma\mu(x/\epsilon)) \quad \text{else} \tag{13}$$

where $\bar{c} = c_0(0)$. The microstructure in the medium is modelled by the random function μ which is a mean zero, stationary stochastic process. We have introduced the small parameter ϵ that distinguishes phenomena occuring on different scales. The random fluctuations in the wave speed takes place on the fast spatial scale x/ϵ and we assume that the microstructure is small, $\sigma = \mathcal{O}(\sqrt{\epsilon})$, in magnitude. The deterministic function $c_0(x)$ models the smooth background variations, corresponding to 'mountain' structures in the water depth. Note that in practice we do not know the details of the medium variations, the μ. However, if we know the statistics of the medium fluctuations we shall be able to describe the main or accumulated effect they have on the propagating pulse.

We consider a wave pulse that comes from the left homogeneous halfspace and is impinging upon the random medium. We want to describe it at some location x. Let the pulse be centered at $x = 0$ at the initial time $t = 0$ (see Figure 2). Consider first the deterministic case with $c(x) \equiv c_0(x)$. The pulse arrives at location x at time $T(x)$ with pulse shape f:

$$\eta(x, T(x) + s) = f(s/\epsilon), \tag{14}$$

$$T(x) = \int_0^x c_0^{-1}(s)ds. \tag{15}$$

Note that we let the pulse be supported on the scale corresponding to the scale of variation of the medium fluctuations. How can we describe the pulse in the random case when $\mu \neq 0$? Observe first that in this case the arrival time at location x becomes random. We will observe the pulse at the random time:

$$\tau(x) = \int_0^x \frac{1 + \sigma\mu(s/\epsilon)/2}{c_0(s)}ds. \tag{16}$$

The modification in the pulse *shape* due to the random medium fluctuations is to leading order *deterministic* [19]. The pulse shaping or modification in the pulse shape can be described via a convolution with the pulse shaping function $\mathcal{H}$:

$$\Psi(x, \tau(x) + s) = \int f(s/\epsilon - u)\mathcal{H}_x(u)du = [f \star \mathcal{H}_x](s/\epsilon), \tag{17}$$

with

$$\mathcal{H}_x(u) = \frac{1}{2\pi}\int e^{-x\omega^2\hat{\gamma}(x,\omega)}e^{-i\omega u}d\omega,$$

$$\hat{\gamma}(x,\omega) = \frac{\int_0^\infty \gamma(s)e^{i\omega s(2/c_0(x))}ds}{4c_0^2(x)},$$

$$\gamma(s) = \frac{\sigma^2}{\epsilon}E[\mu(0)\mu(s)],$$

where E denotes expectation. This result corresponds to (34) in the next section. The derivation of these results can be found in Section 2.1 of [19]. We see that the change in the transmitted pulse shape depends only on the statistics of the medium fluctuations. The description (17) can be simplified in two ways.

First, it follows from the central limit theorem that in distribution

$$\tau(x) \approx \bar{T}(x) + \sigma\int_0^x \frac{1}{2c_0(s)}\mu(s/\epsilon)ds = \bar{T}(x) + \epsilon\,\mathcal{N}(x) \tag{18}$$

where $\mathcal{N}(x)$ is a centered Gaussian random variable with variance:

$$V(x) = \frac{\sigma^2}{2\epsilon}\int_0^x c_0^{-2}(s)ds\int_0^\infty \gamma(s)ds \tag{19}$$

and $\bar{T}(x)$ is the effective medium (or average) travel time to location x. Effective medium theory is valid for short propagation distances on the scale of the wavelength, the scale $\mathcal{O}(\epsilon)$, and it corresponds here to replacing the random speed by the effective medium speed. In this effective medium regime there is no pulse shaping. In the regime that we consider, with relatively long $\mathcal{O}(1)$ propagation distances, the microstructure affects the pulse shape. Moreover, the traveltime includes a small random component. From 19 we see that in the regime $\epsilon = \mathcal{O}(\sigma^2)$ this effect is strong and must be accounted for.

Second, if the pulse profile f varies relatively slowly on the microscale, on the scale ϵ, then the pulse shaping function $\mathcal{H}_x(\cdot)$ can be approximated by a Gaussian kernel with variance (second central moment) $V(x)$:

$$\mathcal{H}_x(u) \approx \frac{1}{\sqrt{2\pi V(x)}}e^{-u^2/(2V(x))}. \tag{20}$$

The effect of the random medium fluctuations is that, when we observe the pulse in the frame defined by the travel time of the random medium, we see a deterministic smearing or spreading of the pulse. For a smooth pulse this spreading can be described as a convolution with a Gaussian kernel. Therefore, the pulse shaping appears as a diffusion in the transmitted pulse shape. In the next section we present a formal calculation that leads to the above pulse shaping picture. Then in the Section III we illustrate the pulse shaping numerically using a piecewise discrete medium with the medium fluctuation being independent in each discrete section. We give explicitly the modification in the shape of the transmitted pulse associated with the discrete case in Appendix A.

IV. DISCUSSION OF THE STOCHASTIC WAVE EQUATIONS

We present a formal derivation of the pulse shaping approximation discussed in the previous section. Consider again the wave system (10–11) The flux function solves the scalar wave equation:

$$\Psi_{xx} - c(x)^{-2}\ \Psi_{tt} = 0, \tag{21}$$

where the local wave speed is $c(x) = \sqrt{gh(x)}$. We model the medium fluctuations by

$$\begin{aligned} c^{-2}(x) &= c_0^{-2} && \text{for } \ x < 0 \\ c^{-2}(x) &= c_0^{-2}(1 + \sqrt{\epsilon}\mu(x/\epsilon)) && \text{else.} \end{aligned}$$

For simplicity we take here the background velocity to be constant equal to c_0. The medium fluctuations are modeled by the mean zero, stationay stochastic process μ. The fluctuations takes place on the microscale, the scale ϵ, and are small $\mathcal{O}(\sqrt{\epsilon})$ in magnitude. The medium fluctuations decorrelate rapidly and has a finite correlation length l:

$$l = \int_0^\infty E[\mu(0)\mu(s)]ds < \infty.$$

A. The effective medium

We shall assume that a source wave is coming from the halfspace homogeneous $x < 0$ and is impinging upon the heterogeneous halfspace $x > 0$. In the homogeneous halfspace we can decompose the wave into right and a left propagating wave components:

$$\Psi(x,t) = a\left(\frac{t - x/c_0}{\epsilon}\right) + b\left(\frac{t + x/c_0}{\epsilon}\right). \tag{22}$$

Observe that we let the wave functions be supported on the microscale, the scale ϵ on which the medium fluctuates. The incoming source wave is given by a and b is the reflected wave. We denote the shape of the incoming source wave by f:

$$a\left(\frac{t}{\epsilon}\right) = f\left(\frac{t}{\epsilon}\right) \tag{23}$$

and assume that f is compactly supported. If the wave travels a distance into the random medium that is on the order of its support then it is not affected by the randomness to leading order. In this case we can replace the random medium by an averaged or **effective medium** defined by the constant wave velocity c_0. That is, we replace $c(x)^{-2}$ in (21) by c_0^{-2}, see for instance [1]. However, we shall consider propagation distances of $\mathcal{O}(1)$. In this case the effects of the randomness builds up and the wave pulse becomes strongly effected by the random fluctuations. In the previous section we described the effects of this interaction and we next give a heuristic derivation that explain the result detailed above.

B. Transformation into right and left traveling waves

We define the Fourier transform, scaled relative to the microscale, by:

$$\check{\Psi}(x,\omega) = \int e^{i\omega s/\varepsilon}\Psi(x,s)\frac{ds}{\epsilon}. \tag{24}$$

From (22) it follows that we can write for $x < 0$

$$\check{\Psi} = \hat{a}e^{i\omega x/\varepsilon c_0} + \hat{b}e^{-i\omega x/\varepsilon c_0}$$

with

$$\hat{a} = \hat{a}(\omega) = \int e^{i\omega t} a(t) dt$$
$$\hat{b} = \hat{b}(\omega) = \int e^{i\omega t} b(t) dt.$$

For $x \in \mathbb{R}$ me make thus the ansatz

$$\check{\Psi}(x,\omega) = \hat{a}(x,\omega) e^{i\omega x/\varepsilon c_0} + \hat{b}(x,\omega) e^{-i\omega x/\varepsilon c_0} \tag{25}$$
$$0 = \hat{a}_x(x,\omega) e^{i\omega x/\varepsilon c_0} + \hat{b}_x(x,\omega) e^{-i\omega x/\varepsilon c_0}, \tag{26}$$

which corresponds to a decomposition into locally right ($\hat{a}$) and left ($\hat{b}$) going wave components when we center with respect to the effective medium frame of reference.

C. Stochastic couping equations

We substitute (25) in (21) and make use of (26) to find the following stochastic coupling equations

$$\frac{d\hat{a}}{dx} = \frac{i\omega\mu}{2c_0\sqrt{\epsilon}}[\hat{a} + \hat{b}e^{-i\omega 2x/\epsilon c_0}] \tag{27}$$
$$\frac{d\hat{b}}{dx} = \frac{-i\omega\mu}{2c_0\sqrt{\epsilon}}[\hat{a}e^{i\omega 2z/\epsilon c_0} + \hat{b}].$$

In the deterministic medium with $\mu = 0$ there is no coupling between the wave components. The random medium modulation μ introduce a coupling between the wave components which is described by the off-diagonal terms in (27). The diagonal terms in (27) give a random correction to the local speed of propagation. To compensate for this we make the following change of variables

$$\alpha^\epsilon(x,\omega) = \hat{a}(x,\omega) e^{-i\omega \int_0^x \mu ds/(\sqrt{\epsilon}2c_0)}$$
$$\beta^\epsilon(x,\omega) = \hat{b}(x,\omega) e^{i\omega \int_0^x \mu ds/(\sqrt{\epsilon}2c_0)}$$

to obtain the amplitude equations

$$\frac{d\alpha^\epsilon}{dz} = \frac{i\omega\mu}{\sqrt{\epsilon}2c_0} \beta^\epsilon e^{-i\omega 2\tau^\epsilon(x)/\epsilon} \tag{28}$$
$$\frac{d\beta^\epsilon}{dz} = -\frac{i\omega\mu}{\sqrt{\epsilon}2c_0} \alpha^\epsilon e^{i\omega 2\tau^\epsilon(x)/\epsilon} \tag{29}$$

with

$$\tau^\epsilon(x) = x/c_0 + \sqrt{\epsilon}\int_0^x \mu(s/\epsilon) ds/(2c_0) = x/c_0 + \chi(x). \tag{30}$$

The random variable $\chi(x)$ corresponds to a small travel time correction. By computing its variance we easily find that it is small $\mathcal{O}(\epsilon)$. Note that α^ϵ and β^ϵ now corresponds to amplitudes in a random frame of reference. They are "centered" with respect to the frame τ^ϵ that is slightly different from the one moving with effective medium speed c_0. The **random** travel time centering makes the system (28) purely "off-diagonal". In the effective medium approximation we ignore the stochastic coupling between the amplitudes, that is, the coupling due to the off-diagonal terms in (28). As we show in the next section, this coupling causes a small modulation of the pulse which becomes appreciable for long propagation distances, in our scaling a propagation distances of $\mathcal{O}(1)$.

D. Averaging of random coupling

We make use of the radiation condition

$$\lim_{x\to\infty} \beta^\epsilon(x,\omega) = 0$$

to obtain from (29) the integral expression

$$\beta^\epsilon(x,z) = \int_x^\infty \frac{i\omega}{\sqrt{\epsilon}2c_0}\mu\left(\frac{s}{\epsilon}\right)\alpha^\epsilon(s,\omega)e^{i\omega 2\tau^\epsilon(s)/\epsilon}\,ds$$

for the reflected amplitude. Moreover, from (28), we then obtain the integro-differential equation

$$\frac{d\alpha^\epsilon}{dz} = \frac{-\omega^2}{4c_0^2}\int_x^\infty \mu\left(\frac{x}{\epsilon}\right)\mu\left(\frac{s}{\epsilon}\right)\alpha^\epsilon(s,\omega)e^{i\omega 2(\tau^\epsilon(s)-\tau^\epsilon(x))/\epsilon}\,ds \tag{31}$$

for the transmitted wave amplitude. Note that in the effective medium the wave amplitude is constant. Thus, we expect only a slow modulation of the amplitude in the random medium. The medium modulation μ, however, vary and decorrelate on the microscale ϵ. We make therefore the approximation

$$\begin{aligned} &E\left\{\int_0^\infty \alpha^\epsilon(\mathrm{x},\omega)\mu\left(\frac{\mathrm{x}}{\epsilon}\right)\mu\left(\frac{\mathrm{s}}{\epsilon}\right)\mathrm{e}^{\mathrm{i}\omega 2(\tau^\epsilon(\mathrm{s})-\tau^\epsilon(\mathrm{x}))/\epsilon}\,\mathrm{ds}/\epsilon\right\} \qquad (32)\\ &\approx E(\alpha^\epsilon(\mathrm{x},\omega))\int_0^\infty \gamma\left(\frac{|\mathrm{x}-\mathrm{s}|}{\epsilon}\right)\mathrm{e}^{\mathrm{i}\omega 2(\mathrm{s}-\mathrm{x})/\epsilon\mathrm{c}_0}\,\mathrm{ds}/\epsilon = \hat{\gamma}(2\omega/\mathrm{c}_0)\mathrm{E}(\alpha^\epsilon(\mathrm{x},\omega)) \end{aligned}$$

in the small ϵ limit, where we defined

$$\begin{aligned} \hat{\gamma}(\omega) &= \int_0^\infty \gamma(s)e^{i\omega s}ds\\ \gamma(v) &= E(\mu(\mathrm{s})\mu(\mathrm{s}+\mathrm{v})). \end{aligned}$$

The full justification of the validity of this step is complicated, see for instance [1]. Making the above approximation in (31) we arrive at the following expression for the mean amplitude in the small ϵ limit

$$\frac{d\alpha}{dx} = \frac{-\omega^2}{4c_0^2}\hat{\gamma}(2\omega/c_0)\alpha, \tag{33}$$

where we used the notation

$$\alpha(x,\omega) = \lim_{\epsilon\to 0} E(\alpha^\epsilon(\mathrm{x},\omega)).$$

E. Approximation for transmitted wave

We use the expression (33) to obtain an approximation for the transmitted wave in the small ϵ limit, we find

$$\begin{aligned} \alpha(x,\omega) &= \alpha(0,\omega)e^{-\omega^2\hat{\gamma}(2\omega/c_0)x/4c_0^2}\\ &= \hat{f}(\omega)e^{-\omega^2\hat{\gamma}(2\omega/c_0)x/4c_0^2}. \end{aligned}$$

If we substitute this approximation for the transformed amplitude for the right propagating mode in the expression for the flux function at depth L we obtain:

$$\begin{aligned} \Psi(L,t) &\approx \frac{1}{2\pi}\int \alpha(L,\omega)e^{i\omega(\tau^\epsilon(L)-t)/\epsilon}d\omega\\ &= \frac{1}{2\pi}\int \hat{f}(\omega)e^{-\omega^2\hat{\gamma}(2\omega/c_0)L/4c_0^2}e^{i\omega(\tau^\epsilon(L)-t)/\epsilon}d\omega \qquad (34)\\ &= [f(\cdot)*\mathcal{H}_L]\left(\frac{t-\tau^\epsilon(L)}{\epsilon}\right) \end{aligned}$$

with

$$\mathcal{H}_L(s) = \frac{1}{2\pi}\int e^{-i\omega t}e^{-\omega^2\hat{\gamma}(2\omega/c_0)L/4c_0^2}d\omega$$

and $*$ being convolution. It is shown in for instance [1] that indeed

$$\lim_{\epsilon\to 0} E(\Psi(\mathrm{L},\tau^\epsilon(\mathrm{L})+\epsilon \mathrm{s}) = [f(\cdot) * \mathcal{H}_L](s). \tag{35}$$

This is the O'Doherty-Anstey pulse-shaping approximation and we refer to $\mathcal{H}$ as the pulse-shaping function. Thus, if we observe the transmitted pulse at a random arrival time we see a mean pulse shape that is obtained as the pulse shape in the effective medium convolved with a pulse shaping function. This function is defined in terms of the correlation function of the medium fluctuations. The source pulse is supported on the same scale as that of the random fluctuations in the medium and the correlation function of these determines the evolution in the pulse shape. We next motivate that not only the mean of the transmitted flux function, but the flux function itself is well approximated by the expression (35).

F. Stabilization

A key aspect of the O'Doherty-Anstey theory is that in the above **random time frame** the flux function Ψ itself is described asymptotically by a **deterministic** shape. Define the variance

$$\begin{aligned} &E([\Psi(\mathrm{L},\tau^\epsilon(\mathrm{L})+\varepsilon \mathrm{s}) - \mathrm{E}(\Psi(\mathrm{L},\tau^\epsilon(\mathrm{L})+\varepsilon \mathrm{s}))]^2) \\ &\sim \frac{1}{(2\pi)^2}\int\int e^{-i(\omega_1+\omega_2)s}\{E[\alpha^\epsilon(\mathrm{L},\omega_1)\alpha^\epsilon(\mathrm{L},\omega_2)] - \alpha(\mathrm{L},\omega_1)\alpha(\mathrm{L},\omega_2)\}\mathrm{d}\omega_1\mathrm{d}\omega_2 \qquad \text{as} \quad \epsilon\downarrow 0. \end{aligned}$$

We introduce the notation

$$\zeta^\epsilon(x,\omega) = \frac{i\omega\mu(x/\epsilon)}{2c_0} e^{-i\omega 2\tau^\epsilon(x)/\epsilon}$$

and find

$$\begin{aligned} \frac{dE[\alpha^\epsilon(x,\omega_1)\alpha^\epsilon(x,\omega_2)]}{dx} = -\int_x^\infty &\{E[\zeta^\epsilon(\mathrm{x},\omega_1)\overline{\zeta^\epsilon(\mathrm{s},\omega_1)}\alpha^\epsilon(\mathrm{s},\omega_1)\alpha^\epsilon(\mathrm{x},\omega_2)] \\ &+ E[\zeta^\epsilon(\mathrm{x},\omega_2)\overline{\zeta^\epsilon(\mathrm{s},\omega_2)}\alpha^\epsilon(\mathrm{x},\omega_1)\alpha^\epsilon(\mathrm{s},\omega_2)]\}\ \mathrm{ds}. \end{aligned}$$

Therefore, if we again make an assumption about 'locality' as in (32) we find

$$E[\alpha^\epsilon(x,\omega_1)\alpha^\epsilon(x,\omega_2)] \sim h(x,\omega_1,\omega_2) \qquad as \quad \varepsilon\downarrow 0,$$

with h solving for for $x>0$

$$\frac{dh}{dx}(x,\omega_1,\omega_2) = -\frac{\omega_1^2\hat{\gamma}(2\omega_1)+\omega_2^2\hat{\gamma}(2\omega_2)}{4c_0^2}h(z,\omega_1,\omega_2).$$

The above argument indeed suggests that $\Psi(L,\tau^\epsilon(L)+\epsilon s) \sim E(\Psi(\mathrm{L},\tau^\epsilon(\mathrm{L})+\epsilon \mathrm{s}))$ in mean square in the limit of ϵ small. This is the remarkable stabilization aspect of the O'Doherty-Anstey theory. The random fluctuations of the pulse when observed in the appropriately *random* time-frame is negligible for small ε, thus, Ψ is described asymptotically by a *deterministic* pulse shape that is a modification of the pulse in the effective medium case through convolution with a pulse shaping function, here denoted $\mathcal{H}$.

The random travel time correction corresponds to observing the transmitted wave relative to the first arrival time defined by

$$T_L = \int_0^L \frac{1}{c(x)}ds = \int_0^L \frac{\sqrt{1+\sqrt{\epsilon}\mu}}{c_0}ds.$$

That is, we can write:

$$\Psi(L,T_L+\varepsilon s) \sim [f(\cdot) * \tilde{H}](s) \qquad as \quad \varepsilon\downarrow 0,$$

with $\tilde{\mathcal{H}}$ being the deterministic causal pulse shaping function defined relative to the first arrival time. In the case that the medium fluctuations define a Markov random process the pulse shaping function $\tilde{H}$ can be interpreted as the distribution of a random sum, [19], and it can be computed explicitly. Assume the exponential correlation function:

$$E(\mu(0)\mu(s)) = Ce^{-s/r}$$

and introduce the non-dimensionalized variables: $\mathcal{Z} = z[C/(16r)]$, $\mathcal{T} = sc_0/(2r) := s\lambda$. Parameterized in terms of these variables we find that the pulse shaping function is:

$$\tilde{\mathcal{H}}(\mathcal{Z},\mathcal{T}) = \lambda\ e^{-\mathcal{Z}}[\delta(\mathcal{T}) + e^{-\mathcal{T}}\ \sqrt{\mathcal{Z}/\mathcal{T}}\ I_1(\sqrt{\mathcal{Z}\mathcal{T}})],$$

with I_1 being the modified Bessel function of order one.

G. Low frequency limit

A simple characterization of $\mathcal{H}$ can be obtained in the low frequency limit. In this limit we can replace $\hat{\gamma}(2\omega/c_0)$ in (34) by $\hat{\gamma}(0) = l$, we therefore find

$$\Psi(L, \tau^\epsilon(L) + \varepsilon s) \approx [f(\cdot) * \mathcal{N}_L](s) \qquad as\ \ \varepsilon \downarrow 0 \tag{36}$$

where $\mathcal{H}$ is approximated by $\mathcal{N}_L$, a centered Gaussian pulse with variance $V_L = lL/(2c_0^2)$. The travel time correction relative to the effective medium travel time is random and is on the microscale given by $\chi(L)/\epsilon$, with χ defined in (30). The Central Limit Theorem shows that this quantity is approximately a Gaussian random variable with variance V_L.

H. Transmitted wave in effective medium frame of reference

We show how the **mean** of the transmitted wave can be characterized when we observe it in the deterministic time frame defined by the effective medium parameters. It follows from the above results that the transmitted wave for ϵ small and in the low frequency limit can be approximated as

$$\Psi(L, \tau^\epsilon(L) + \varepsilon s) \approx [f(\cdot) * \mathcal{N}_L](s) = (1/2\pi) \int e^{-i\omega s} \hat{f}(\omega) e^{-\omega^2 V_L/2}\ d\omega.$$

If we evaluate the transmitted wave in the effective frame of reference we find:

$$\Psi(L, L/c_0 + \varepsilon s) \approx (1/2\pi) \int e^{-i\omega s} e^{i\omega\chi^\epsilon(L)/\epsilon} \hat{f}(\omega) e^{-\omega^2 V_L/2}\ d\omega$$

with $\chi^\epsilon(L)/\epsilon$ defined by (30). For ϵ small this quantity is approximately a Gaussian random variable with variance V_L. The mean of the pulse in this frame can be obtained by integrating with respect to the density for $\chi^\epsilon(L)/\epsilon$, then we find

$$\begin{aligned} E[\Psi(L, L/c_0 + \epsilon s)] &\approx (1/2\pi) \int\int \hat{f}(\omega)\ e^{-\omega^2 V_L/2}\ e^{-i\omega s}\ \frac{e^{-u^2/2V_L}}{\sqrt{2\pi V_L}}\ e^{i\omega u}\ du\ d\omega \\ &= (1/2\pi) \int \hat{f}(\omega)\ e^{-\omega^2 V_L/2}\ e^{-i\omega s}\ e^{-\omega^2 V_L/2}\ du\ d\omega \\ &= [f(\cdot) * \mathcal{N}_{2V_L}](s). \end{aligned}$$

Hence, the spreding of the mean pulse in this time frame is defined as in (36) only with twice the variance for the pulse shaping function.

V. NUMERICAL ILLUSTRATION WITH SHALLOW WATER WAVES

A. Initial configuration for the numerical simulations

The numerical validation experiments are performed in a configuration as represented in figure 2. The initial wave profile is given by a Gaussian elevation placed over the flat region (left side of figure 2). At the early stages of the simulation a travelling pulse will propagate to the right with unit speed. After a small time interval the pulse starts to interact with the disordered topography. The initial pulse width is effectively one. The topography is 100 units long so that the simulation can capture the asymptotic regime described in the theory. The topography is described

by a slowly varying sinusoidal background, having a disordered layered microstructure as presented in figure 2. The layered microstructure is given by piecewise constant ridges of random height. It is constructed so that the wave speed corresponds to expression (13). In all experiments the background wave speed is

$$c_0^2(x_i) = 1 + 0.3\sin(kx_i).$$

The (mean–zero) heights of the ridges fluctuate by 20% and the ridge-width is 0.1. The parameter k corresponds to the scale of variation of the smooth background medium.

The three-dimensional equations (1–3) are discretized by an implicit, semi–Lagrangian technique [6]. A brief description of the numerical method and benchmark experiments is given in the appendix. All experiments were performed with a one-layer, one-dimensional grid as described below. The shallow water model reduces to the system (4–6). The reason for adopting the current strategy is that the numerical scheme is very efficient and can be extended to experiments in higher dimensions.

The discretization parameters used in the numerical simulations are: 10700 nodes in the x-direction spaced by $\Delta x = 0.01$ and 3 nodes in the y-direction, where 2 are along the solid/impermeable sides of the channel. The topography is located from node 400 up to node 10400. The other nodes are over a flat region. In the vertical direction we use 1 layer. The normalized propagation speed is equal to one and the nonlinearity parameter is $\alpha = 0.3 \cdot 10^{-3}$. The initial Gaussian profile is centered at j=250. To record the transmitted wave at the fixed station (j=10400) we use 43000 time steps of length $\Delta t = 0.0025$.

B. Numerical experiments

We carry out four numerical experiments which illustrate that the solution of the nonlinear equations (4–6) is accurately described by the asymptotic approximation introduced in Section III in the regime of small parameters considered.

Experiment 1: Deterministic diffusion in a random frame

In this first example we show that the transmitted water wave pulse, to leading order, is *deterministic* when observed at its *random* arrival time. We use the model described in the previous section, but with a constant background, that is $k = 0$. Figure 3 shows a detail of one realization of this medium. In Figure 4(A) we show transmitted pulse shapes after propagation over the random ridges in the water bottom. The 25 lines correspond to propagation over different realizations of the random piecewise–constant topography. The transmitted pulses are plotted (in time) at a *fixed station* along the free surface. The station is located 50 units into the random topography and the initial pulse width is unity. At the station we record the water elevation at all times. In the plot we show the observed pulse starting from a fixed time ($t = 19900\Delta t$). Note that the travel time to the station is random. The average travel time for the pulses to the station is the effective medium travel time, see equation (18). In Figure 4(B) we show the same pulses, but now we plot them centered at their random arrival time. When we center the pulses in this way it becomes clear that the apparent diffusion, or broadening of the pulse, caused by the random medium fluctuations, is deterministic and independent of the particular realization. The transmitted pulses are broader than the initial pulse of unit width (i.e. covering 100 gridpoints), since the interaction with the rapid variation in the water depth causes them to diffuse about their center. This broadening is what we refer to as anomalous diffusion and it can be described analytically using the medium statistics as we illustrate next.

Experiment 2: Propagation over largescale bottom ondulations

In this second example we show the pulse shaping in the case where the bachground has a sinusoidal variation (the mean water depth). We use the model introduced in the previous section with a sinusoidal background, using $k = 1/20$.

We first show the transmitted water pulse in the case *without* random fluctuations in the water depth, that is $\sigma = 0$. The topography is exactly as in Figure 5, but without the microstructure. The solid line in Figure 6 displays the free surface elevation as the pulse is reaching the station point. A very mild oscillation is observed behind the pulse. This is due to the slowly varying topography. The initial pulse profile is shown with the dashed line. Note that in the absence of the random microstructure pulse broadening (or apparent diffusion) is not observed.

Next, we consider the case with microstructure and $\sigma = 0.2$. Figure 5 shows a realization of the medium. In this figure we also show the propagating water pulse in order to illustrate the scaling in the problem.

The apparent diffusive effect, due to the ridge-microstructure, is clearly seen in Figure 7 where we plot the transmitted pulse with the solid line. The narrow dashed line is, as above, the initial pulse profile. The dashed line coinciding with the solid line is the prediction of the pulse shaping according to the theory, as in (A5). The theoretical prediction of the pulse shaping is very good.

Experiment 3: Waters with rapid bottom ondulations
We next let the background landscape (i.e. the slowly varying component of the topography) vary on a faster scale. This illustrates the robustness of the theory, which is based on separation of scales. We choose parameters as in the previous example only that the period of the sinusoidal component of the topography is reduced. The period corresponds to 6.5 times the initial pulse's wave length, rather than 20 as above (that is $k = 1/6.5$). We show the transmitted pulse in Figure 8. The agreement between the numerical solution (solid line) and the theoretical prediction of the pulse shaping (dashed line) is still very good.

Experiment 4: Larger fluctuations in the water depth
The final example further illustrates the robustness of the theory. We use the same parameters as in Example 2, only that we now increase the strength of the random fluctuations in the water depth such that the amplitude of the ridge-microstructure is approximately doubled ($\sigma = 0.4$). As expected, the apparent diffusion effect is enhanced as can be seen in Figure 9. Again the agreement with the theoretical prediction shown by the dashed line is very good. Note that the transmitted pulse shape is close to the Gaussian shape. Since the travelling pulse in this example becomes smooth and broad relative to the microstructure the Gaussian approximation in (20) well describes the pulse shaping.

VI. CONCLUSIONS AND FUTURE WORK

We studied the effective behaviour of long coastal waves traveling over rough topographies containing a smooth slowly varying profile together with disordered small-scale features. The main (stochastic theory) asymptotic result is that the medium fluctuations cause the propagating pulse to broaden as it travels. This *apparent diffusion* depends only on the traveling distance and the *statistics* of the random medium fluctuations. Thus, the broadening is described in a deterministic way independently of the particular medium realization. Note that effective medium theory is valid for short propagation distances on the scale of very few wavelengths. In the effective medium regime (i.e. homogenization theory) there is no pulse shaping. In the regime of long propagation distances the microstructure affects the pulse shape.

The robustness of the linear theory was validated numerically for a wide parameter regime through a nonlinear shallow water solver (TRIM3D). We varied both the microscale fluctuation level as well as the horizontal length scales of the topography and obtained very good agreement with the theory.

We are currently working on the diffusive upscaling of the microstructure of the topography. As mentioned in our introduction, the "representation (...) of subgrid-scale orographic processes is recognized as crucial to numerical weather prediction at all time ranges" (ECMWF [8]). We also intend to perform the full validation of the locally layered O'Doherty-Anstey theory, a two-dimensional theory [19]. Furthermore we are working on the extension of the O'Doherty-Anstey theory for weakly dispersive waves.

VII. ACKNOWLEDGEMENTS

We are grateful to George Papanicolaou (Stanford University, USA) for establishing the contact between us and for providing support (through NSF grant DMS97-09320) while we initiated our collaboration at the Mathematical Geophysics Summer School (MGSS1998), which continued through MGSS2000 and MGSS2001, all held at Stanford University.

A. Nachbin would like to thank Vincenzo Casulli (Università di Trento, Italy) for the copy of his 3D hydrostatic Navier–Stokes code (TRIM3D) and Greg Kriegsmann (New Jersey Institute of Technology, USA) for his hospitality and support during a 1998 visit at NJIT which played an important role in getting this project started.

A. Nachbin's work was supported in part by: CNPq under Grant 300368/96-8; CNPq under Grant CNPq/NSF 910029/95-4; and NEC/CEMAT under Grant DMS 2.419/98-00.

K. Sølna's work was supported by the National Science Foundation under Grant No. 0093992.

APPENDIX A: THE DISCRETE PULSE SHAPING FUNCTION

As in Section III we discuss the solution of the wave system (10–11). Here we consider a discrete version of the result (17) that gives the pulse shaping. First, we assume a constant background medium that is uniformly discretized in space. The local speed of sound is:

$$c^2(x) = c_n^2 = c_0^2 \quad \text{for} \quad x < 0 \tag{A1}$$
$$c^2(x) = c_n^2 = c_0^2(1 + \sigma\mu_i) \quad (n-1)\Delta x \ < \ x \ < \ n\Delta x. \tag{A2}$$

The medium fluctuations μ_n are identically, independently distributed random variables bounded above and below: $-1 < a < \mu_n < b$. The μ_i's have zero mean and unit variance. Consider first the deterministic case and let the discrete version of the transmitted pulse be:

$$\Psi(x_n, t_n + i\Delta t) = f_i, \tag{A3}$$

with $x_n = n\Delta x$, $t_n = n\Delta t$ and $\Delta t = \Delta x/c_0$. As above, we let the pulse be centered at the origin for $t = 0$. Consider next the random case and denote the travel time to location x_n by τ_n:

$$\tau_n = \sum_{i=1}^{n} \frac{1}{c_n} \Delta x. \tag{A4}$$

Then, the transmitted pulse can be approximated by

$$\Psi(x_n, \tau_n + i\Delta t) \approx \mathbf{f} \star \tilde{\mathcal{H}}(i) \tag{A5}$$

with $\star$ being discrete convolution. The discrete causal pulse shaping function is:

$$\tilde{\mathcal{H}}_i = 0 \quad \text{for} \quad i < 0 \tag{A6}$$
$$\tilde{\mathcal{H}}_i = p_i \quad \text{else} \tag{A7}$$

with $p_i = e^{-a}a^i/i!$ being the discrete Poisson distribution with parameter $a = n\sigma^2/4$. Note that the smearing of the pulse happens on the scale of the discretization when $n = \mathcal{O}(\sigma^{-2})$. Consider next the case with a variable background:

$$c^2(x) = c(n)^2 = c_0^2(1) \quad \text{for} \quad x < 0 \tag{A8}$$
$$c^2(x) = c(n)^2 = c_0(n)^2(1 + \sigma\mu_i) \quad (n-1)\Delta x \ < \ x \ < \ n\Delta x. \tag{A9}$$

The description (A5) prevails only in that the expression for the parameter a in the Poisson distribution becomes

$$a = \frac{\sigma^2}{4} \sum_{i=1}^{n} (c_0(i)/c_0)^2. \tag{A10}$$

For a large the Poisson distribution becomes approximately the (discrete) Gaussian distribution with expectation a and variance a. Thus, for n large the pulse shaping function $\tilde{\mathcal{H}}$ has approximately the shape of the Gaussian kernel. It can be checked that the expression (19) gives (A10) for the above discrete medium model. Finally, if $n = \mathcal{O}(\sigma^{-2})$ then in distribution

$$\tau_n + a \approx \bar{t}_n + \Delta t \mathcal{N} \tag{A11}$$

with $\bar{t}_n$ being the effective medium travel time to depth x_n and $\mathcal{N}$ being a centered Gaussian random variable with variance a as in (18).

APPENDIX B: NUMERICAL MODEL

The 3D equations are discretized by an implicit, semi–Lagrangian technique which accomplishes the objective that the stability of the scheme does not depend on the celerity. Based on a linear stability analysis Casulli & Cheng [6] derived a scheme which treats implicitly the pressure gradient term ($\nabla\eta$-term) and the velocity terms in the free surface equation. This method is actually called a semi–implicit scheme because, in the full model, the vertical diffusion term is discretized implicitly while the horizontal diffusion discretization is kept explicit.

The spatial grid consists of rectangular cells, centered at (x_i, y_j, z_k), of length Δx, Δy and height Δz_{ijk}^n. This height is interpreted as the thickness of the k-th layer of the 3D grid. Because of the presence of the topography and free surface, this thickness can vary in space and time (indicated by the superscript n). The convection terms are treated in a Lagrangian form, through the discretization of the material derivative $(D/Dt)_{ijk}^n$. A fixed staggered grid is defined on the horizontal planes, at the interface between vertical layers. The numerical transport is performed

in an Eulerian–Lagrangian manner, relying therefore on the interpolation of the respective grid point–values at the backward–characteristic points of departure. Only one layer was used in the experiments presented below. Details are given in Casulli & Cheng [6] and the references within.

To normalize the wave celerity we choose our parameters so that the reference shallow water speed is always equal to one: $(gh_0) = 1$ or $g = 1/h_0$. The implicit scheme constant is taken to be $\theta = 0.5$ (Crank–Nicolson). This value minimizes the numerical dissipation and numerical diffusion is not observed. Several validation experiments were performed in Nachbin [15] and Nachbin & Casulli [16] and the numerical solution exhibited very good conservation properties. In the preliminary numerical experiments (Nachbin & Casulli [16]) it was observed that for the parameter $\alpha = 0.1$ the regime is strongly nonlinear and the waves very quickly break into bores.

---

[1] M. Ash, W. Kohler, G. C. Papanicolaou, M. Postel and B. White, *Frequency content of randomly scattered signals*, SIAM Review, V 33, 519-625, (1991).

[2] Baines, P.G., *Topographic Effects in Stratified Flows*, Cambridge Univ. Press, (1995).

[3] Belzons M., Guazzelli E. and Parodi O., *Gravity waves on a rough bottom: experimental evidence of one-dimensional localization*, J. Fluid Mech., Vol. 186, pp. 539–558, (1988).

[4] Burridge R. and P. Lewicki and G. C. Papanicolaou, *Pulse stabilization in a strongly heterogeneous layered medium*, Wave Motion, V 20, 177-195, (1994).

[5] Burridge R., G. C. Papanicolaou and B. White, *One dimensional wave propagation in a highly discontinuous medium*, Wave Motion, V 10, 19-44, (1988).

[6] Casulli, V., and Cheng, R.T., *Semi-implicit finite difference methods for three-dimensional shallow water flow*, Int. J. Num. Meth. Fluids, vol. 15, pp. 629–648, (1992).

[7] Devillard P., Dunlop F. and Souillard B., *Localization of gravity waves on a channel with a random bottom*, J. Fluid Mech., Vol. 186, pp. 521–538, (1988).

[8] European Centre for Medium-Range Weather Forecasts (ECMWF), *Orography*, Proceedings of a Workshop held at ECMWF, (1998).

[9] Clouet J. F. and J. P. Fouque, *Spreading of a pulse travelling in random media.*, Annals of Applied Probability, V 4, 1083-1097, (1994).

[10] R. Dashen, W. H. Munk, K. M. Watson and F. Zachariasen, *Sound transmission through a fluctuating ocean*, Editor S. Flatte, Cambridge University Press, 1979.

[11] Lewicki P., *Long time evolution of wavefronts in random media*, SIAM J. Appl. Math., V 54, 907-934, (1994).

[12] Lewicki P., R. Burridge and M. V. de Hoop, *Beyond Effective Medium Theory: Pulse Stabilization for Multimode Wave Propagation in High Contrast Layered Media.*, SIAM Journal on Applied Math., V 56, 256-276, (1996).

[13] Mei C. C. *The applied dynamics of ocean surface waves*, John Wiley, (1983).

[14] Nachbin A., *The localization length of randomly scattered water waves*, J. Fluid Mech., V 296, 353-372, (1995).

[15] Nachbin A., *The effective behaviour of linear and nonlinear waves in irregular channels*, IMPA Preprint Série A2001/91, (2001).

[16] Nachbin A. and V. Casulli, Water waves: linear potential theory results validated with a hydrostatic Navier-Stokes model, In: Mathematical and Numerical Aspects of wave Propagation, Editor J. A. DeSanto, SIAM, (1998).

[17] Nachbin A. and G. Papanicolaou, *Water waves in shallow channels of rapidly varying depth*, J. Fluid Mech., V 241, 311-332, (1992).

[18] O'Doherty R. F. and N. A. Anstey, *Reflections on amplitudes*, Geophysical Prospecting, V. 19, 430-458, (1971).

[19] Papanicolaou G. and K. Sølna, *Ray theory for a locally layered random medium*, Waves in Random Media, V. 151-198, (2000).

[20] Sølna K., *Stable spreading of acoustic pulses due to laminated microstructure*, Thesis, Stanford University, (1997).

[21] Sølna K., *Estimation of pulse shaping for well logs*, to appear in Geophysics, (2001).

[22] Whitham G. B. *Linear and nonlinear waves*, John Wiley, (1974).

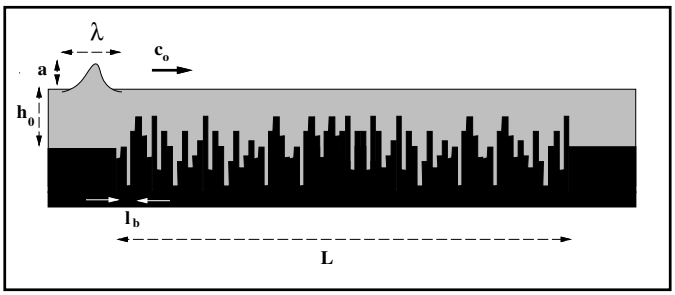

FIG. 1. Schematic figure with typical length scales.

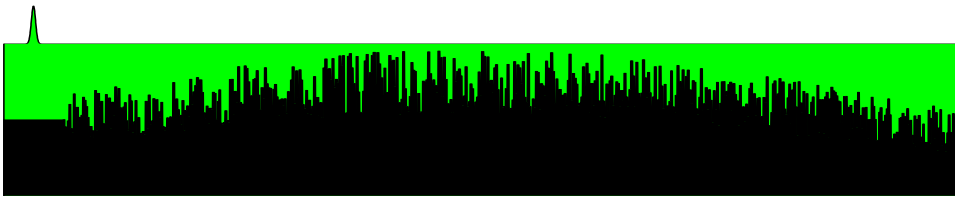

FIG. 2. Detail of the left-end of the long propagation region. The vertical scale of the rightgoing pulse has been exagerated.

FIG. 3. Detail of the random component of the topography.

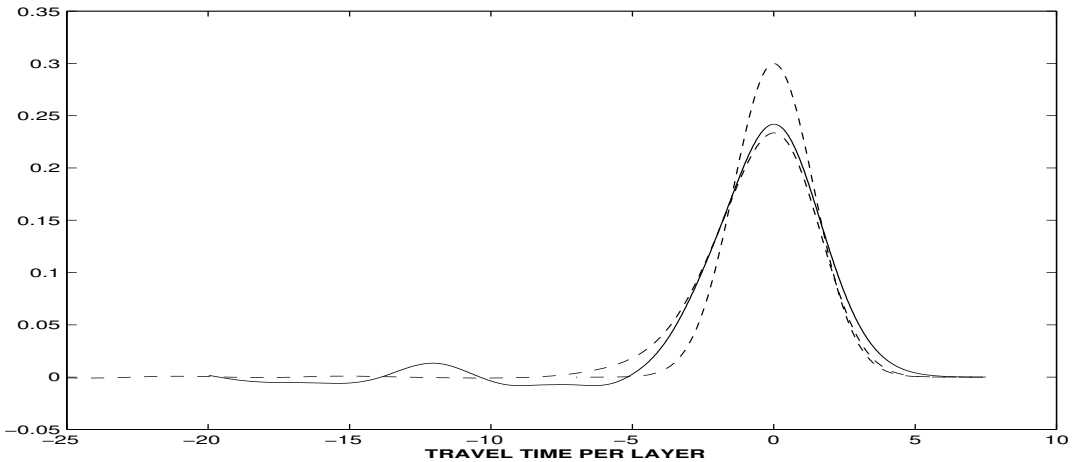

FIG. 4. The transmitted pulse shape, obtained by propagating a Gaussian pulse over different realizations of the synthetic topographies. **(A)** The solid lines correspond to 25 different realizations of the topography. Note that the travel time up to this fixed station is random. It takes more than $20000\Delta t$'s to reach this station. **(B)** All 25 wave profiles are centered at the origin. The pulse shaping is seen to be deterministic.

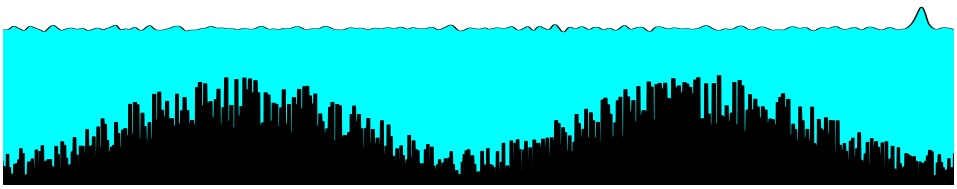

FIG. 5. Detail of the transmitted and reflected waves over the locally layered topography.

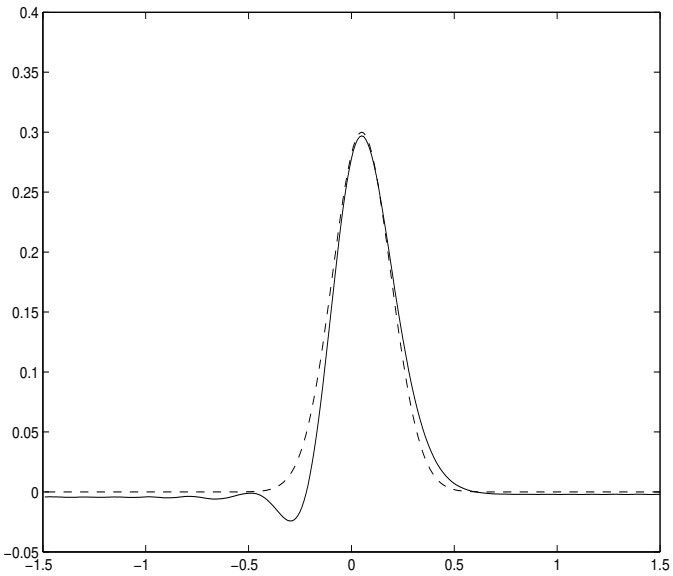

FIG. 6. Gaussian pulse after propagating over a slowly varying sinusoidal topography (solid line). The dashed line is the initial condition. Both were centered at the origin for comparison.

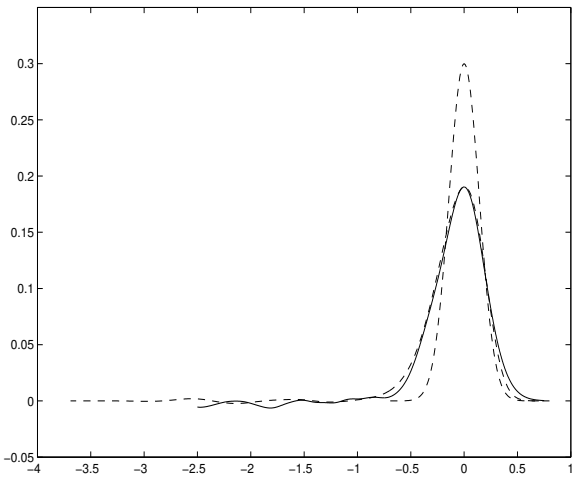

FIG. 7. The solid line represents the numerical solution. The higher pulse (dashed line) represents the pulse's initial profile. The broader dashed line represents the pulse shaping theory. Waves centered at the origin for comparison.

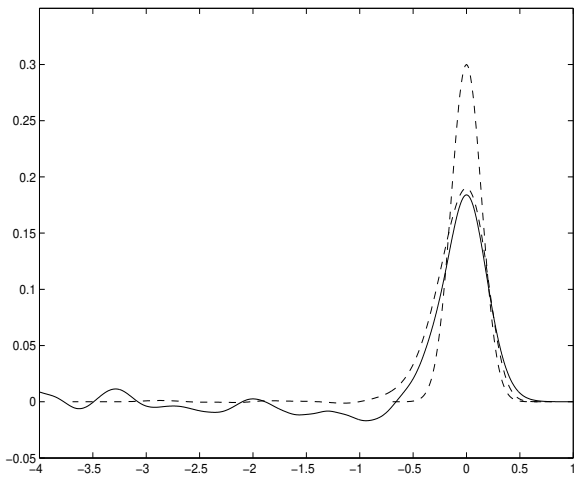

FIG. 8. The solid line represents the numerical solution. The higher pulse (dashed line) represents the pulse's initial profile. The broader pulse (dashed line) represents the pulse shaping theory. The period of the sinusoidal background variation in the water depth is about 1/3 of its value in Figure 7.

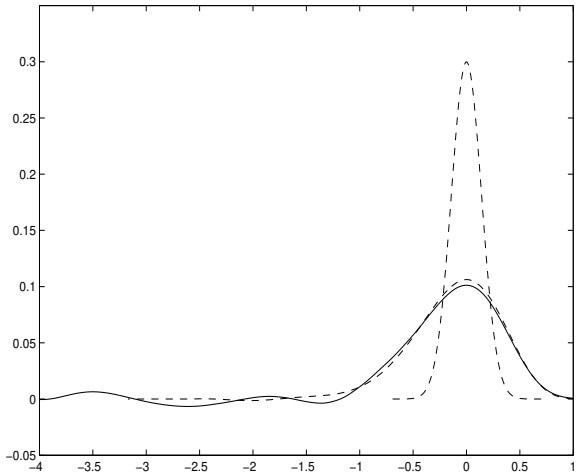

FIG. 9. The solid line represents the numerical solution. The higher pulse (dashed line) represents the pulse's initial profile. The broader pulse (dashed line) represents the theoretical prediction. The microstructure's amplitude is twice as large as in Figure 7.